3+2+X: What is the most useful depolarization input for retrieving microphysical properties of non-spherical particles from lidar measurements by assuming spheroidal particle shapes?

Matthias Tesche[1,2,*], Alexei Kolgotin[3], Moritz Haarig[4], Sharon P. Burton[5], Richard A. Ferrare[5], Chris A. Hostetler[5], and Detlef Müller[1]

[1]School of Physics, Astronomy and Mathematics, University of Hertfordshire, Hatfield, United Kingdom
[2]now at Leipzig Institute for Meteorology (LIM), Leipzig University, Leipzig, Germany
[3]A. M. Prokhorov General Physics Institute, Moscow, Russia
[4]Leibniz Institute for Tropospheric Research (TROPOS), Leipzig, Germany
[5]NASA Langley Research Center, Hampton, USA

Correspondence to: Matthias Tesche (matthias.tesche@uni-leipzig.de)

Abstract. The typical multiwavelength aerosol lidar data set for inversion of optical to microphysical parameters is composed of three backscatter coefficients (β) at 355, 532, and 1064 nm and two extinction coefficients (α) at 355 and 532 nm. This data combination is referred to as $3\beta+2\alpha$ or 3+2 data set. This set of data is sufficient for retrieving some important microphysical particle parameters if the particles have spherical shape. Here, we investigate the effect of including the particle linear depo-
5   larization ratio (δ) as a third input parameter to the inversion of lidar data. The inversion algorithm is generally not used if measurements show values of δ that exceed 0.10 at 532 nm, i.e. in the presence of non-spherical particles such as desert dust, volcanic ash, and under special circumstances biomass-burning smoke. We use experimental data collected with instruments that are capable of measuring δ at all three lidar wavelengths with an inversion routine that uses the theory of light scattering by randomly oriented spheroids to replicate scattering properties of non-spherical particles. This is the first systematic test of the
10 effect of using all theoretically possible combinations of δ taken at 355, 532, and 1064 nm as input in the lidar data inversion.

We find that depolarization information at least at one wavelength already provides useful information in the inversion of optical data that describe light-scattering by non-spherical particles. However, any choice of δ_λ will give lower values of the single-scattering albedo than the traditional 3+2 data set. We find that input data sets that include δ_{355} give a non-spherical fraction that closely resembles the dust ratio we obtain from using β_{532} and δ_{532} in a methodology applied in aerosol-type
15 separation. The use of δ_{355} in data sets of two or three δ_λ reduces the fraction of non-spherical particles that is retrieved when using δ_{532} and δ_{1064}. Use of the latter two without accounting for δ_{355} generally leads to high fractions of non-spherical particles that we consider not trustworthy. The use of three δ_λ instead of two δ_λ including the constraint that one of these is measured at 355 nm does not provide any advantage over using 3+2+δ_{355}. We conclude that — depending on measurement capability — the future standard input for inversion using spheroid kernels might be 3+2+δ_{355} or 3+2+δ_{355}+δ_{532}.

1 Introduction

Over the past two decades, the inversion of multiwavelength aerosol lidar measurements for the retrieval of aerosol microphysical properties (*Müller et al.*, 1998, 1999a, b, 2001; *Veselovskii et al.*, 2002; *Ansmann and Müller*, 2005) matured to a stage that allows for automated and unattended data processing (*Müller et al.*, 2014). The methodology uses multiwavelength lidar

5 measurements of aerosol backscatter and extinction coefficients (i.e. the availability of a $3\beta+2\alpha$ input data set, also referred to as 3+2 data set) and the mathematically correct description of light scattering by small particles to solve the ill-posed inverse problem at hand (*Ansmann and Müller*, 2005). Mie theory is used for the mathematical description of light scattering by particles. By definition, this theory cannot be applied to describe light scattering by non-spherical particles. This causes a problem, as aerosol types such as mineral dust or volcanic ash are of non-spherical shape.

10 The presence of such non-spherical particles in lidar measurements is identified by non-zero values of the particle linear depolarization ratio (δ, *Gimmestad* 2008). Spherical particles do not depolarize the emitted laser light, and thus, show values of δ close to zero. Depolarization-ratio measurements with advanced lidars (*Freudenthaler et al.*, 2009) allow for the retrieval of the contribution of non-spherical particles to the measured intensive optical parameters (*Tesche et al.*, 2009b; *Burton et al.*, 2014), and thus allow for comprehensive aerosol-type characterization (*Burton et al.*, 2012; *Groß et al.*, 2013).

15 A data base for light-scattering by non-spherical particles (Dubovik model, *Dubovik et al.* 2006) developed for the inversion of sun-photometer measurements within the framework of the Aerosol Robotic Network (AERONET, https://aeronet.gsfc.nasa.gov/, *Holben et al.* 1998) has been implemented in the lidar data inversion algorithm used here. The first application of the Dubovik model to lidar measurements of mineral dust has been presented by *Veselovskii et al.* (2010), *Di Girolamo et al.* (2012), *Papayannis et al.* (2012), and *Müller et al.* (2013). *Veselovskii et al.* (2010) performed inversions with the non-spherical light-

20 scattering data base on the basis of the traditional 3+2 input data set as well as a 3+2+1 data set that uses δ_{532} as additional input. The latter parameter can provide information on the contribution of mineral dust to the total aerosol optical properties. From the comparison of the inversion runs with the different input data sets, the authors conclude that using 3+2+1 provides no advantage over the conventional 3+2 input run in which the non-spherical fraction is set a priori to 100%. They attribute this insensitivity (with regard to the use of δ_{532}) to the fact that (i) the Dubovik model had not been specifically designed for lidar

25 applications, i.e. the mathematical description of light scattering at 180°, and (ii) that high values of δ_{532} can only be obtained for values of particle refractive indices that are below values found from atmospheric observations (*Veselovskii et al.*, 2010). *Papayannis et al.* (2012) present results of the inversion of 3+2 data in the presence of mineral dust while *Di Girolamo et al.* (2012) and *Müller et al.* (2013) used 3+2+1 data sets with depolarization information at 355 nm and 532 nm, respectively. *Veselovskii et al.* (2016) present results of the inversion of lidar data for mineral dust for the case of the conventional 3+2 input

30 (with non-spherical fraction set to 100%) and the 3+2+1 input with depolarization information at 532 nm. The authors conclude that it is currently not possible to come to a definitive conclusion as to which input data set leads to a more accurate estimation of dust parameters. Instead, they recommend to use the 3+2 input for measurements of pure dust as these inversions provide more realistic estimations of the refractive index of dust particles. Because scattering kernels based on Mie theory cannot

represent light scattering by non-spherical particles, i.e. particles that increase δ_λ, another way to circumvent the problem is to extract the information related to non-spherical particles from the optical input (*Tesche et al.*, 2009b, 2011b).

On the one hand, the answer to the question of which inversion input provides the most accurate estimate of dust microphysical parameters requires independent measurements of these parameters. An example for such a study is presented by *Müller et al.* (2013). However, the comprehensive data sets required for such an effort can only be obtained in the framework of dedicated and extensive experiments. On the other hand, there has yet been no systematic estimation of the effect of using different depolarization input for the inversion of lidar data. Today, depolarization-ratio profiling is most commonly performed at 532 nm. This explains the use of this wavelength in the studies of *Veselovskii et al.* (2010, 2016) and *Müller et al.* (2013). This wavelength is also the only one for which comparisons of the algorithm performance of using the 3+2 and the 3+2+1 data set exists. For a future standard on depolarization-ratio profiling it is crucial to assess which wavelength provides the best prospects not only for aerosol characterization but also for using the added information as input to inversion runs. Most inversions that use the Dubovik model focused on pure-dust conditions. Values of δ_{532} were similar to values observed close to dust source regions (*Freudenthaler et al.*, 2009). Such conditions warrant the use of the 3+2 data set with the non-spherical fraction set to 100%. It yet needs to be investigated if depolarization information also allows for the successful retrieval of aerosol microphysical properties in mixed layers of mineral dust and other spherical aerosol types, i.e. aerosol scenarios that are common for observations of long-range transport of mineral dust in the free troposphere. Finally, the latest developments of realizing depolarization-ratio profiling at 1064 nm or multiple wavelengths (*Burton et al.*, 2015; *Haarig et al.*, 2017a) leads to the question if these new measurement capabilities might also advance the quality of the inversion of lidar measurements in the presence of non-spherical particles.

In this study, we investigate the effect of using δ at 355, 532, and 1064 nm as additional inversion input to answer the question:

> *What is the optimum choice of δ_λ in the inversion of lidar measurements of non-spherical particles described by randomly oriented spheroids?*

We address this question with the use of 3+2+3 multiwavelength lidar measurements taken under both pure and mixed-dust conditions. Specifically, we assume that values of δ_λ are accurate within their respective measurement error and that the findings of this studies are primarily related to the light-scattering model used in the inversion calculations. We start the paper with an overview of the data sources and inversion setup in Section 2. The results are presented and discussed in Sections 3 and 4, respectively. We close with a summary and our conclusions in Section 5.

2   Data and methods

This section provides an overview of the lidar data used in this study as well as a brief description of the inversion procedure.

2.1 Lidar data

To date, few lidar instruments have the capability to measure 3+2+3 data sets and we refer to *Burton et al.* (2015), *Haarig et al.* (2017a), and *Hu et al.* (2018). Here, we use data of (1) the NASA Langley Research Center's High Spectral Resolution Lidar 2 (HSRL-2) that has been operated aboard the NASA B-200 King Air aircraft in the framework of the DISCOVER-AQ project

5 (https://discover-aq.larc.nasa.gov/) and (2) the Backscatter Extinction lidar-Ratio Temperature Humidity profiling Apparatus (BERTHA) of the Leibniz Institute for Tropospheric Research (TROPOS) taken during the Saharan Aerosol Long-range Transport and Aerosol-Cloud-Interaction Experiment (SALTRACE, *Weinzierl et al.* 2017).

HSRL-2 is the second-generation airborne HSRL developed at NASA Langley Research Center. It builds on the heritage of the HSRL-1 system (*Hair et al.*, 2008) but operates at the laser wavelengths of 355, 532, and 1064 nm. The 3+2+3 data

10 collected with HSRL-2 allow for a comprehensive characterization of different aerosol types (*Burton et al.*, 2012) and the retrieval of microphysical particle properties *Müller et al.* (2014). Further details on the instrument can be found in *Müller et al.* (2014) and *Burton et al.* (2018).

DISCOVER-AQ measurements with HSRL-2 were screened for observations that showed elevated levels of δ_{532}. The observations were identified as dusty mix (*Burton et al.*, 2012) and include flights during DISCOVER-AQ California 2013 (2 cases),

15 DISCOVER-AQ Texas 2013 (4 cases), and DISCOVER-AQ Colorado 2014 (3 cases). An overview of the DISCOVER-AQ measurement days considered here is given in Table 1. The optical input data for the inversion were obtained in the first step by averaging temporally over several minutes of measurements and in the second step by carrying out data averaging over height layers of 150 m.

3+2+3 measurements with TROPOS' BERTHA lidar during SALTRACE are used to assess the performance of the different

20 inversion input data sets in the presence of pure dust conditions. This test under pure dust conditions is needed as such a scenario was not encountered during DISCOVER-AQ.

While BERTHA had been used to characterize the optical properties of pure dust during the Saharan Mineral Dust Experiment (SAMUM, *Tesche et al.* 2009b), the capability of carrying out triple-wavelength δ measurements with BERTHA has only recently been presented in *Haarig et al.* (2017a). So far, such measurements have been performed to characterize mineral dust

25 (*Haarig et al.*, 2017a), marine aerosols (*Haarig et al.*, 2017b), and biomass-burning smoke (*Haarig et al.*, 2018). An overview of the SALTRACE measurement days considered here is given in Table 1.

2.2 Inversion of lidar data

The inversion of multiwavelength lidar data is based on using light-scattering kernels that were computed on the basis of Mie theory (*Ansmann and Müller*, 2005). *Veselovskii et al.* (2010) were the first to investigate the possibility of using non-spherical

30 scattering kernels computed for randomly oriented spheroids (*Dubovik et al.*, 2006). This study and those of *Müller et al.* (2013) and *Veselovskii et al.* (2016) added the δ at 532 nm to the input data. The information provided by δ allows for retrieving the non-spherical particle fraction as an additional inversion output parameter. For instance, *Müller et al.* (2013) obtained non-spherical fractions close to 100% under conditions of pure Saharan dust as identified by $\delta_{532} \geq 0.31$.

Because depolarization-ratio measurements at 532 nm are most common (*Pappalardo et al.*, 2014; *Baars et al.*, 2016), it will be the first choice of the new standard input for the lidar inversion using non-spherical kernels (*Veselovskii et al.*, 2010, 2016). In this paper, we investigate if this input is sufficient for retrieving (some of) the microphysical parameters or if improved results can be obtained by adding depolarization information at 355 and/or 1064 nm (*Gasteiger and Freudenthaler*, 2014).

5   Inversion calculations have been performed with eight base functions and by varying the minimum and maximum particle radius of the inversion window between 0.075 and 0.450 μm and 0.1 and 10.0 μm, respectively. The real part of the refractive index was varied between 1.3 and 1.6 with steps of 0.05 while the imaginary part of the refractive index was set to cover a range from 0 to 0.03 in steps of 0.005. The non-spherical fraction was varied between 0% and 100% in steps of 10%. A non-spherical fraction of 100% means that calculations are performed using exclusively non-spherical kernels (i.e. the Dubovik model) while

10 a value of 0% refers to using Mie kernels. This setup leads to a total of 3675 solutions per inversion run. In the analysis of the inversion calculations, we have averaged those 140 to 200 solutions that revealed the smallest discrepancy to the optical input data.

Standard inversion outputs are particle number, surface, and volume concentration, effective radius derived from these parameters, complex refractive index, and single-scattering albedo (SSA). The inversion with spheroid kernels also provides us

15 with an estimate of the contribution of non-spherical particles to the values we obtain for each of the parameters.

For the measurements listed in Table 1, inversion runs have been performed with depolarization input ranging from zero to three wavelengths. We obtain eight runs per measurement height bin. An overview of the various combinations and the name of each data set is given in Table 2. The current standard input 3+2 data sets do not account for depolarization information (Set I).

20 ## 3   Results

We present selected measurement cases that illustrate the effect of the choice of inversion input data set on the retrieved aerosol microphysical properties. These case studies describe scenarios of varying concentration of non-spherical particles. We then discuss the results for the entire data set outlined in Table 1.

3.1   Example: pure dust

25 A 3+2+3 measurement conducted with BERTHA on 20 June 2014 during SALTRACE, Barbados (*Haarig et al.*, 2017a; *Weinzierl et al.*, 2017) has been chosen. This case represents nearly pure dust conditions, i.e. a situation dominated by non-spherical particles, and has previously been decribed in *Mamouri and Ansmann* (2017). The profiles of β, α, and δ are shown in Figure 1. High values of δ of about 0.26 at 532 nm and 0.24 at 355 and 1064 nm and wavelength-independent values of α (extinction-related Ångström exponent of zero, not shown) and lidar ratios of 40 to 55 sr (not shown) are indicative of nearly

30 pure dust conditions Similar values were observed during SAMUM (*Tesche et al.*, 2009b, 2011a). The circles in the plots of the backscatter and extinction coefficients mark the data that were used as input for the inversion, i.e. 11 sets at 11 height levels between 1.0 and 4.0 km height. The mean δ_{532} for this height range is 0.26. This value results in a dust fraction of 0.83

with regard to the backscatter coefficient at 532 nm, according to the method described by *Tesche et al.* (2009b). While higher dust fractions would be desirable to properly represent pure-dust conditions (see, e.g. *Freudenthaler et al.* 2009), the general scarcity of suitable measurement data means that this is the "purest" 3+2+3 dust case available to us at the time of this study.

Figure 2 shows the results we obtained from the inversion of the eight depolarization-related variations of input data (see Ta-

5 ble 2). We show the results for the effective radius, the 532-nm SSA, the non-spherical fraction, and the volume concentration. The inversion of all input data sets shows a decrease of effective radius and volume concentration with height. Little difference is visible in the inversion results for these parameters apart from the slight variation of Set I. We obtain a much clearer separation between the inversion results for Set 1 (the traditional 3+2 data set) and Sets II to VIII (which include depolarization information) for the SSA and the non-spherical fraction. The high values of δ_{532} lead to a dust fraction above 80% (dashed

10 line in Figure 2c). Unsurprisingly, Set I is the only one that does not result in a very large fraction of non-spherical particles. In fact, non-spherical particle fractions were never found to exceed 40% when using the traditional 3+2 input regardless of the dust content in the mixed pollution plumes. A similar non-spherical fraction of on average 35% has previously been reported for the inversion of 3+2 data sets obtained for Saharan dust (*Veselovskii et al.*, 2010). The unrealistic values of non-spherical particles obtained for Set I coincide with SSA values of as low as 0.82. That value is much lower than the values we obtain for

15 the other sets. SSA is slightly lower for measurement cases that include δ_{355} (Sets II, V, VI, and VIII), compared to cases that do not include depolarization information at 355 nm (Sets III, IV, and VII). Overall, input data sets that include depolarization information give similar output data for the case of pure dust conditions.

3.2 Example: mixed dust

Figure 3 shows a measurement taken with HSRL-2 on 25 September 2013 in the framework of DISCOVER-AQ Texas. The

20 data present the average of eight minutes of measurement time, i.e. between 2057 and 2105 UTC. This measurement case provides more insight on the sensitivity of data products on optical input data that were taken under mixed dust conditions, i.e. a situation in which mineral dust is mixed with spherical particles and depolarization values are below the ones generally observed for pure dust. The column aerosol load during this measurement was rather low as indicated by an aerosol optical thickness (AOT) of 0.16 at 532 nm (see Table 1).

25 The 3+2+3 profiles in Figure 3 show aerosols in a well-mixed layer up to a height of 2.4 km. The mean value of δ_{532} is 0.099. This number translates to a dust mixing ratio of 0.346 (Table 1, *Burton et al.* (2012)). The strong wavelength dependence of the backscatter and extinction coefficients suggests the presence of small particles caused by combustion processes. The Houston area is influenced by the oil industry and high volume of traffic. The increased values of δ_{532} are an indicator for the presence of mineral dust. Consequently, dusty mix and urban/pollution were identified as most abundant aerosol types during

30 the measurement (*Burton et al.*, 2012). However, Figure 3 also shows a strong wavelength dependence of the values of δ_λ, i.e. we find lower (higher) values at 355 nm (1064 nm) compared to 532 nm. This indicates that the choice of wavelength of the depolarization ratio could potentially influence the retrieval.

Figure 4 shows the result of the inversion of the optical data represented by the colored circles in Figure 3. As for the case of pure dust, the volume-concentration profile follows the shape (profile) of the extensive parameters, i.e. backscatter and

extinction coefficient. The lowest values of volume concentration are obtained for the case in which δ_{532} is used as additional information in data inversion. The highest values are found for inversions that make use of the full set of δ_λ, i.e. the 3+2+3 data set. Taking into consideration the profiles from all eight inversion runs, however, reveals that the choice of depolarization input seems to have no major effect on particle volume concentration – particularly not on the shape of the profile. In fact, we

5 find comparably small differences of the values of volume concentration for the different input data sets that are defined by a variable number of depolarization information.

In contrast, the use of a different number of depolarization information results in a much stronger spread of the non-spherical fraction. If we use no depolarization information we obtain spheroid fractions that vary between 20% and 30% and change erratically from height bin to height bin. The sets III, IV, and VII (i.e. those with δ_{532}, δ_{1064}, and $\delta_{532} + \delta_{1064}$) result in rather

10 high non-spherical fractions between 75% and 90%. This result seems to be a clear overestimate as such conditions would refer to the dominance of mineral dust. This predominance is in disagreement with the dust fraction presented in Figure 3. The most plausible spheroid fractions of around 40% combined with strong vertical homogeneity are found for input data sets that contain δ_{355}, i.e. sets II, V, VI, and VIII. These values are also closest to the mean dust ratio of 0.35 that has been determined from the optical data (see Table 1). The profile follows the profile of the dust ratio (dashed line in Figure 4) quite closely.

15 The separation of the results for different input data can also be seen in the profiles of SSA at 532 nm, see Figure 4b. Data sets that show higher non-spherical fractions also coincide with SSA values that are up to 0.02 higher than values obtained from optical data sets that include information on δ_{355}. This study mainly targets the comparison of results we obtain from using different combinations of depolarization information. We consider the values of the non-spherical fraction more realistic and consider data sets that use δ_{355} as more trustworthy than data sets that do not include depolarization information at 355 nm.

20 ## 3.3 General findings

Figure 5 presents two cases for which the choice of depolarization input has a profound effect on the retrieved non-spherical fraction. In the case of 13 July 2014, the steady decrease of δ_λ with height translates to a similar decrease of the non-spherical fraction, but only for data sets that include δ_{355}. In fact, this decrease closely follows the decrease of dust fraction with height. As for the previous cases, no variation with height is found when using the traditional 3+2 data set. Sets III, IV, and VII, all of

25 which are lacking depolarization information at 355 nm, do not result in non-spherical fractions smaller than 80%. The case of 17 July 2014 is even more striking as – in contrast to the previous examples – δ is low at all wavelengths and the dust fraction obtained from the optical data is actually zero. Despite this clear pattern of the optical data, the inversion of the different input data sets gives a wide range of non-spherical fractions: below 20% for Sets II, V, VI, and VIII; slightly higher values of up to 30% in the lower half of the aerosol layer for Set I; values between 40% and 70% for Sets III and VII; and more than 70% for

30 Set IV. This outcome suggests that using δ_{1064} does not improve the performance of our particular inversion method using the spheroid Dubovik model. This result is in contrast to the results presented by *Gasteiger and Freudenthaler* (2014). While δ_{1064} certainly does provide additional informational content, this cannot be exploited when combining the Dubovik model with the inversion algorithm used in this study.

A more complete picture of the effect of the choice of δ_λ on the retrieved non-spherical fraction is provided in Figure 6. The figure includes all 156 data points obtained from the cases listed in Table 1. The results we obtain from the eight inversion runs is split according to data sets that include, respectively do not include δ_{355}. As in the case of the examples shown before, we consider the retrieved non-spherical fraction as the microphysical manifestation of the optically-derived dust ratio (*Tesche et al.*, 2009b). Figure 6 clearly shows that only input data sets that include δ_{355} lead to any meaningful correlation between dust ratio and non-spherical fraction. The parameters of the linear regressions presented in Figure 6 are listed in the bottom half of Table 2. The steepest slope and largest values of the squared correlation coefficients are found for Sets V and VIII, i.e. the sets that either use input values for δ_λ at 355 and 532 nm or all $3\delta_\lambda$, respectively. Figure 6b confirms that (i) non-spherical fractions above 40% are impossible to obtain from traditional 3+2 data sets, (ii) the data sets with δ_{1064} give non-spherical fractions that are poorly correlated to the obtained dust ratios, and (iii) data sets that include δ_{532} but not δ_{355} result in increased non-spherical fractions that increase with increasing dust ratio but rarely stay below 40%. We therefore conclude from Figure 6 that δ_{355} has a regulating effect on the inversion output and that data sets that include δ_{355} are generally more trustworthy (certainly with respect to the non-spherical fraction) than those that do not include δ_{355}.

In the following, we are hence contrasting the results for the volume concentration, the effective radius, and the SSA according to the two sub-sets of Figure 6a and b. We want to find out if these parameters differ within and between these two groups. The difference between using 3+2+1 and 3+2+2 input data sets from the two groups (i.e. with and without δ_{355}) is shown in Figure 7 for volume concentration, effective radius, and 532-nm SSA. The correlation between Sets II and III and between Sets V and VII shows little difference for the effective radius. The use of 3+2+2 input data generally gives larger volume concentration but again little difference is found between the data sets considered in this work. The strongest effect with regard to the choice of input data is found for the SSA. Input data that include δ_{355} tend to give lower values of SSA; see for example Figures 2 and 4. Figure 7c shows a range between 0.94 and 0.98 for Sets II and V whereas we find a considerably narrower range from 0.96 to 0.98 for Sets III and VII.

Figure 8 is analogous to Figure 7 but now compares volume concentration, effective radius, and SSA within the two groups identified in Figure 6. Again, the choice of input data set has the smallest effect on effective radius and volume concentration, though the latter is systematically lower for Set II compared to Sets V, VI, and VIII. We don't find a similar effect in cases that exclude δ_{355} but still include information on particle depolarization. For the SSA, any inversion that considers δ_{355} seems to give similar results. We find the same pattern for data sets that exclude δ_{355} as long as any depolarization input is considered. All inversion input that include some depolarization information generally give higher SSA values than the traditional 3+2 data set.

4 Discussion

The non-spherical model of *Dubovik et al.* (2006) has been developed for application to sun photometer measurements in the framework of AERONET. This model marks a considerable advance when compared to treating light-scattering by non-spherical particles with Mie theory. However, this light-scattering model considers rather simplified particle shapes, i.e. ro-

tational symmetric spheroids with a defined axis-ratio distribution which might not be suitable to reproduce all of the light-scattering properties of non-spherical particles in the atmosphere. Indeed, comparisons to independent in-situ measurements and lidar observations of Saharan dust during SAMUM have revealed discrepancies for the retrieved complex refractive index and single-scattering albedo (*Müller et al.*, 2013). In addition, the intensive lidar parameters lidar ratio and particle linear de-

5 polarization ratio, which can be calculated from the inferred scattering matrix, do not agree with coincident measurements at the 355- and 532-nm lidar wavelengths (*Müller et al.*, 2013).

Shin et al. (2018) present spectral lidar ratios and particle linear depolarization ratios representative for mineral dust from different source regions. The authors used the AERONET data base of level 2.0 sun photometer inversions. They find the best agreement to lidar observations of both parameters at the longer wavelengths of 870 and 1020 nm. Towards shorter wavelengths,

10 the AERONET-derived values show an increase of the lidar ratio and a decrease of the particle linear depolarization ratio. Both spectral behaviours are not found in lidar measurements of mineral dust (*Freudenthaler et al.*, 2009; *Shin et al.*, 2018). Other models that employ more realistic geometries of non-symmetric non-spherical particles have been developed for use in lidar applications (*Gasteiger et al.*, 2011). These models suggest improvements in inferring aerosol microphysical properties from lidar data by using measurements of δ_{1064} in the inversion (*Gasteiger and Freudenthaler*, 2014). However, such alternatives

15 generally lack the flexibility of the Dubovik model when it comes to their implementation for new applications. In addition, there are still enormous challenges involved in testing these alternatives in view of the complexity of particle shapes and the computational resources required for running simulation studies.

The results we obtain from our study are somewhat contradictory to the findings of *Gasteiger and Freudenthaler* (2014) and *Shin et al.* (2018) who attribute the greatest informational value and representativeness to observations of δ_{1064}. We have

20 performed the first systematic investigation of the effect of all possible combinations of depolarization-related inversion input at the wavelengths of 355, 532, and 1064 nm on the retrieved aerosol microphysical properties. Particularly the retrieved fraction of non-spherical particles needed to reproduce the measured optical properties leads us to the conclusion that measurements of either δ_{355} only or depolarization-ratio measurements at several wavelengths in which one of the parameters is δ_{355} provide the most useful addition to the 3+2 data set for the inversion of lidar data using this methodology that have been collected

25 in the presence of non-spherical particles. We emphasize again that this finding refers to using Dubovik's model of randomly oriented spheroids for the description of light-scattering by non-spherical particles in this inversion algorithm.

Our findings provide insights that go beyond previous studies on the effect of adding depolarization information to the inversion of multiwavelength lidar data:

1. Previous studies focused exclusively on pure-dust situations, i.e. values of δ_{532} of 0.30 (*Veselovskii et al.*, 2010, 2016;

30 *Müller et al.*, 2013). These studies showed that the depolarization ratio should not be used as input for the inversion of dust particle parameters. Instead, the inversion should be performed with 3+2 input and the non-spherical fraction manually set to 100%. Our results show that this conclusion may have been driven by using δ_{532}. Our study shows that δ_{532} may not be an ideal input parameter.

2. We present the first inversion results for lidar observations of mixtures of spherical and non-spherical particles of varying degree and varying spectral behaviour of the particle linear depolarization ratio. Considering such conditions rather than only pure-dust cases allows for using the retrieved non-spherical particle fraction as an additional indicator for the quality of the inversion results.

3. We present the first systematic (though relational) study of the effect of the choice of depolarization input based on actual atmospheric triple-depolarization-ratio measurements. Previous investigations of the effect of depolarization input on the inversion results have been restricted to using either δ_{355} (*Di Girolamo et al.*, 2012) or δ_{532} (*Veselovskii et al.*, 2010, 2016; *Papayannis et al.*, 2012; *Müller et al.*, 2013), and thus, could relate the findings only to the results of using the conventional 3+2 input data set. The lack of spectral depolarization-ratio measurements under dusty conditions neither allowed for investigating how the choice of input parameters affects the quality of inversion results compared to benchmark data nor test if the choice is ideal.

4. Following in the footsteps of AERONET, microphysical particle properties mark the next logical data product level in the analysis of multiwavelength aerosol lidar data. It is therefore of vital importance to define the minimum information needed for this purpose (i.e. the best choice of input data) as this decision relates directly to the optimum setup for lidar instruments whose measurements can provide this data product. This study represents an important step for determining that information. The main issue in that regard is weighting the benefits of using instrument setups which are already highly challenging over the added information provided by these measurements. This decision-making is of particular importance in light of future spaceborne lidar missions that will focus on aerosol profiling as well as their airborne demonstrators.

Veselovskii et al. (2010, 2016) use the complex refractive index in their argumentation of their preference of rejecting the depolarization input in the inversion. They retrieve real parts of about 1.45 for pure dust, which are comparable to AERONET results. They conclude that imaginary parts obtained from the inversion of 3+2 input data lead to more realistic estimations of this parameter because values below 0.005 (derived from using 3+2+1) are below the findings from in-situ measurements (*Müller et al.*, 2013). Our preliminary analysis of the refractive index shows real parts of 1.50 to 1.55 for all combinations of depolarization input for both mixed- as well as pure-dust conditions (not shown). This result is more in line with independent measurements of this parameter (*Müller et al.*, 2013). For pure dust conditions we obtain imaginary parts of up to 0.020 from the inversion of 3+2 data sets. All other sets lead to significantly lower values. For mixed-dust cases in which $\delta_{532} < 0.25$, we find significantly larger imaginary parts that show little difference to the results of using the 3+2 input data set.

5 Summary and conclusions

We have performed a first systematic relational investigation of the effect of using different combinations of depolarization information in the context of using it as additional input to the inversion of optical lidar data into aerosol microphysical properties. In this work, we use 3+2+3 measurements obtained with the NASA LaRC HSRL-2 during DISCOVER-AQ and the

TROPOS BERTHA during SALTRACE — two out of just three instruments currently capable of measuring δ_λ simultaneously at all three wavelengths generally used in aerosol profiling with lidar.

We have selected eleven observations. Increased values of δ_{532} can be used as a proxy for the presence of an increased concentration of mineral dust in atmospheric layers. Eight sets of optical data have been created for each of the individual

5 measurements. Depolarization input ranged from zero to three wavelengths. We focused on a relational study in view of the challenges connected to (i) using the AERONET light-scattering model that currently provides the best possible output results for sun photometer observations and (ii) the lack of light-scattering models that are proven to work for the special condition of observing non-spherical particles at 180-degree observation angle (lidar configuration). We are comparing the output of the different inversion runs to each other and to the dust ratio obtained from the optical data. In that way we want to identify the

10 most plausible results.

We find that inversion without depolarization information (i.e. the traditional 3+2 data set) cannot lead to non-spherical particle fractions larger than 40% even if non-spherical kernels, i.e. the spheroid Dubovik model, are used. We also find that the use of depolarization ratios at 532 or 1064 nm in combination with the Dubovik model give unrealistically high non-spherical particle fractions. These fractions generally exceed the dust ratio inferred from the measurements of β_{532} and δ_{532}

15 following the procedure described by *Tesche et al.* (2009a). While it needs to be emphasized that the non-spherical fraction as inferred from the inversion is an artificial, non-physical parameter, it might be considered as the ratio of the concentration of dust to total particle concentration. The most realistic non-spherical fractions is found when using depolarization information at 355 nm.

The choice of depolarization input was found to have little effect on the retrieval of extensive parameters such as the volume

20 concentration and the effective radius that can be derived from this extensive parameter. The use of depolarization input at any wavelength, i.e. 355 nm or 532 nm or 1064 nm, generally increases the retrieved values of the 532-nm SSA compared to the 3+2 input. Our hypothesis is that the use of depolarization information leads to a lower value of the imaginary part compared to the inversion in which the traditional 3+2 data set is used. Consequently SSA increases. We conclude that any choice of input data to microphysical inversion using the Dubovik model is acceptable as long as it contains δ_{355}. However, we do not find a

25 significant advantage of using three δ over using δ at fewer wavelengths. This result leads us to conclude that the most suitable input data set for lidar inversion using spheroid kernels is 3+2+1 in which we use δ_{355}.

We investigated the connection between output of inversions for different sets of input data. Definite conclusions can only be drawn if coincident independent in-situ data were available for the considered cases. An alternative approach to circumvent any reliance on the accuracy of the non-spherical fraction would be to separate the optical input data according to the contributions

30 of spherical and non-spherical particles (*Tesche et al.*, 2009a, 2011b) before running the inversion with non-spherical fractions set to zero and unity, respectively. In any case, the use of spheroids for approximating light-scattering by non-spherical particles is limited for lidar applications (*Müller et al.*, 2013) and new models with more realistic particle geometries (*Kahnert et al.*, 2014; *Nousiainen and Kandler*, 2015) will be needed to accurately link microphysical properties to the optical parameters measured with advanced aerosol lidars (*Gasteiger et al.*, 2011). It is quite possible that such improved light-scattering models will

35 show better skill in extracting the informational content provided by particle linear depolarisation ratios at 532 and 1064 nm.

Data availability. DISCOVER-AQ data are publicly available from the Science Team at the NASA Atmospheric Science Data Center (ASDC) via doi:10.5067/Aircraft/DISCOVER-AQ/Aerosol-TraceGas. SALTRACE data are available from M. Haarig upon request.

Author contributions. MT, DM, and AK had the idea for this study and performed the inversion runs. SPB, RAF and CAH collected the HSRL-2 data during DISCOVER-AQ. MH collected the BERTHA data during SALTRACE. MT performed the analysis and interpretation

5   of the inversion data and prepared the figures. All authors contributed to the discussion of the findings and the preparation of the manuscript.

Competing interests. The authors declare that no competing interests are present.

Acknowledgements. This activity is supported by ACTRIS Research Infrastructure (EU H2020-R&I) under grant agreement no. 654109.

References

Ansmann, A. and D. Müller (2005), Lidar and atmospheric aerosol particles, in *LIDAR—Range-resolved optical remote sensing of the atmosphere*, edited by C. Weitkamp, pp. 105-141, Springer, New York, NY, USA.

Baars, H., Kanitz, T., Engelmann, R., Althausen, D., Heese, B., Komppula, M., Preißler, J., Tesche, M., Ansmann, A., Wandinger, U., Lim, J.-H., Ahn, J. Y., Stachlewska, I. S., Amiridis, V., Marinou, E., Seifert, P., Hofer, J., Skupin, A., Schneider, F., Bohlmann, S., Foth, A., Bley, S., Pfüller, A., Giannakaki, E., Lihavainen, H., Viisanen, Y., Hooda, R. K., Pereira, S. N., Bortoli, D., Wagner, F., Mattis, I., Janicka, L., Markowicz, K. M., Achtert, P., Artaxo, P., Pauliquevis, T., Souza, R. A. F., Sharma, V. P., van Zyl, P. G., Beukes, J. P., Sun, J., Rohwer, E. G., Deng, R., Mamouri, R.-E., and Zamorano, F.: An overview of the first decade of PollyNET: An emerging network of automated Raman-polarization lidars for continuous aerosol profiling, Atmos. Chem. Phys., 16, 5111-5137, https://doi.org/10.5194/acp-16-5111-2016, 2016.

Burton, S. P., Ferrare, R. A., Hostetler, C. A., Hair, J. W., Rogers, R. R., Obland, M. D., Butler, C. F., Cook, A. L., Harper, D. B., and Froyd, K. D.: Aerosol classification using airborne High Spectral Resolution Lidar measurements – methodology and examples, Atmos. Meas. Tech., 5, 73-98, https://doi.org/10.5194/amt-5-73-2012, 2012.

Burton, S. P., Vaughan, M. A., Ferrare, R. A., and Hostetler, C. A.: Separating mixtures of aerosol types in airborne High Spectral Resolution Lidar data, Atmos. Meas. Tech., 7, 419-436, https://doi.org/10.5194/amt-7-419-2014, 2014.

Burton, S. P., Hair, J. W., Kahnert, M., Ferrare, R. A., Hostetler, C. A., Cook, A. L., Harper, D. B., Berkoff, T. A., Seaman, S. T., Collins, J. E., Fenn, M. A., and Rogers, R. R.: Observations of the spectral dependence of linear particle depolarization ratio of aerosols using NASA Langley airborne High Spectral Resolution Lidar, Atmos. Chem. Phys., 15, 13453-13473, https://doi.org/10.5194/acp-15-13453-2015, 2015.

Burton, S. P., Hostetler, C. A., Cook, A. L., Hair, J. W., Seaman, S. T., Scola, S., Harper, D. B., Smith, J. A., Fenn, M. A., Ferrare, R. A., Saide, P. E., Chemyakin, E. V., and Müller, D.: Calibration of a high spectral resolution lidar using a Michelson interferometer, with data examples from ORACLES, Appl. Opt., 57, 6061-6075, https://doi.org/10.1364/AO.57.006061, 2018.

DISCOVER-AQ Science Team, Hampton, VA, USA: NASA Atmospheric Science Data Center (ASDC), Accessed 03/09/2018 at doi:10.5067/Aircraft/DISCOVER-AQ/Aerosol-TraceGas

Di Girolamo, P., Summa, D., Bhawar, R., Di Iorio, T., Cacciani, M., Veselovskii, I., Dubovik, O., and Kolgotin, A.: Raman lidar observations of a Saharan dust outbreak event: characterization of the dust optical properties and determination of particle size and microphysical parameters, Atmos. Environ., 50, 66-78, 2012.

Dubovik, O., Sinyuk, A., Lapyonok, T., Holben, B. N., Mishchenko, M., Yang, P., Eck, T. F., Volten, H., Muñoz, O., Veihelmann, B., van der Zande, W. J., Léon, J.-F., Sorokin, M., and Slutsker, I.: Application of spheroid models to account for aerosol particle nonsphericity in remote sensing of desert dust, J. Geophys. Res., 111, D11208, https://doi.org/10.1029/2005JD006619, 2006.

Freudenthaler, V., Esselborn, M., Wiegner, M., Heese, B., Tesche, M., Ansmann, A., Müller, D., Althausen, D., Wirth, M., Fix, A., Ehret, G., Knippertz, P., Toledano, C., Gasteiger, J., Garhammer, M., and Seefeldner, M.: Depolarization ratio profiling at several wavelengths in pure Saharan dust during SAMUM 2006, Tellus, 61B, 165–179, https://doi.org/10.1111/j.1600-0889.2008.00396.x, 2009.

Gasteiger, J., Wiegner, M., Groß, S., Freudenthaler, V., Toledano, C., Tesche, M., and Kandler, K.: Modeling lidar-relevant optical properties of complex mineral dust aerosols, Tellus B, 63, 725–741, https://doi.org/10.1111/j.1600-0889.2011.00559.x, 2011.

Gasteiger, J. and Freudenthaler, V.: Benefit of depolarization ratio at $\lambda = 1064\,\mathrm{nm}$ for the retrieval of the aerosol microphysics from lidar measurements, Atmos. Meas. Tech., 7, 3773-3781, https://doi.org/10.5194/amt-7-3773-2014, 2014.

Gimmestad, G. G.: Reexamination of depolarization in lidar measurements, Appl. Optics, 47, 3795-3802, https://doi.org/10.1364/AO.47.003795, 2008.

Groß, S., Esselborn, M., Weinzierl, B., Wirth, M., Fix, A., and Petzold, A.: Aerosol classification by airborne high spectral resolution lidar observations, Atmos. Chem. Phys., 13, 2487-2505, https://doi.org/10.5194/acp-13-2487-2013, 2013.

5   Haarig, M., Ansmann, A., Althausen, D., Klepel, A., Groß, S., Freudenthaler, V., Toledano, C., Mamouri, R.-E., Farrell, D. A., Prescod, D. A., Marinou, E., Burton, S. P., Gasteiger, J., Engelmann, R., and Baars, H.: Triple-wavelength depolarization-ratio profiling of Saharan dust over Barbados during SALTRACE in 2013 and 2014, Atmos. Chem. Phys., 17, 10767-10794, https://doi.org/10.5194/acp-17-10767-2017, 2017a.

Haarig, M., Ansmann, A., Gasteiger, J., Kandler, K., Althausen, D., Baars, H., Radenz, M., and Farrell, D. A.: Dry versus wet marine particle
10   optical properties: RH dependence of depolarization ratio, backscatter, and extinction from multiwavelength lidar measurements during SALTRACE, Atmos. Chem. Phys., 17, 14199-14217, https://doi.org/10.5194/acp-17-14199-2017, 2017b.

Haarig, M., Ansmann, A., Baars, H., Jimenez, C., Veselovskii, I., Engelmann, R., and Althausen, D.: Depolarization and lidar ratios at 355, 532, and 1064 nm and microphysical properties of aged tropospheric and stratospheric Canadian wildfire smoke, Atmos. Chem. Phys., 18, 11847-11861, https://doi.org/10.5194/acp-18-11847-2018, 2018.

15   Hair, J. W., Hostetler, C. A., Cook, A. L., Harper, D. B., Ferrare, R. A., Mack, T. L., Welch, W., Izquierdo, L. R., and Hovis, F. E.: Airborne high-spectral-resolution lidar for profiling aerosol optical profiles, Appl. Opt., 47, 6734-6752, https://doi.org/10.1364/AO.47.006734, 2008.

Holben, B. N., Eck, T. F., Slutsker, I., Tanré, D., Buis, J., Setzer, A., Vermote, E., Reagan, J., Kaufman, Y. J., and Nakajima, T.: AERONET—A federated instrument network and data archive for aerosol characterization, Rem. Sens. Environ., 66, 1-16, https://doi.org/10.1016/S0034-
20   4257(98)00031-5, 1998.

Hu, Q., Goloub, P., Veselovskii, I., Bravo-Aranda, J.-A., Popovici, I., Podvin, T., Haeffelin, M., Lopatin, A., Pietras, C., Huang, X., Torres, B., and Chen, C.: A study of long-range transported smoke aerosols in the Upper Troposphere/Lower Stratosphere, Atmos. Chem. Phys. Discuss., https://doi.org/10.5194/acp-2018-655, in review, 2018.

Kahnert, M., Nousiainen, T., and Lindqvist, H.: Review: Model particles in atmospheric optics, J. Quant. Spectrosc. Rad. Trans., 146, 41-58,
25   http://dx.doi.org/10.1016/j.jqsrt.2014.02.014, 2014.

Mamouri, R.-E. and Ansmann, A.: Potential of polarization/Raman lidar to separate fine dust, coarse dust, maritime, and anthropogenic aerosol profiles, Atmos. Meas. Tech., 10, 3403-3427, https://doi.org/10.5194/amt-10-3403-2017, 2017.

Müller, D., Wandinger, U., Althausen, D., Mattis, I., and Ansmann, A.: Retrieval of physical particle properties from lidar observations of extinction and backscatter at multiplewavelengths, Appl. Opt., 37, 2260–2263, 1998.

30   Müller, D., Wandinger, U., and Ansmann, A.: Microphysical particle parameters from extinction and backscatter lidar data by inversion with regularization: Theory, Appl. Opt., 38, 2346–2357, 1999a.

Müller, D., Wandinger, U., and Ansmann, A.: Microphysical particle parameters from extinction and backscatter lidar data by in-version with regularization: Simulation, Appl. Opt., 38, 2358–2368, 1999b.

Müller, D., Wandinger, U., Althausen, D., and Fiebig, M.: Comprehensive particle characterization from three-wavelength Raman-lidar
35   observations, Appl. Opt., 40, 4863-4869, 2001.

Müller, D., Ansmann, A., Freudenthaler, V., Kandler, K., Toledano, C., Hiebsch, A., Gasteiger, J., Esselborn, M., Tesche, M., Heese, B. and Althausen, D.: Mineral dust observed with AERONET Sun photometer, Raman lidar, and in situ instruments during SAMUM 2006: Shape-dependent particle properties, J. Geophys. Res., 115, https://doi.org/10.1029/2009JD012523, 2010.

Müller, D., Veselovskii, I., Kolgotin, A., Tesche, M., Ansmann, A., and Dubovik, O.: Vertical profiles of pure dust (SAMUM-1) and mixed smoke-dust plumes (SAMUM-2) inferred from inversion of multiwavelength Raman/polarization lidar data and comparison to AERONET retrievals and in-situ observations, Appl. Optics, 52, 3178-3202, https://doi.org/10.1364/AO.52.003178, 2013.

Müller, D., Hostetler, C. A., Ferrare, R. A., Burton, S. P., Chemyakin, E., Kolgotin, A., Hair, J. W., Cook, A. L., Harper, D. B., Rogers, R. R., Hare, R. W., Cleckner, C. S., Obland, M. D., Tomlinson, J., Berg, L. K., and Schmid, B.: Airborne Multiwavelength High Spectral Resolution Lidar (HSRL-2) observations during TCAP 2012: vertical profiles of optical and microphysical properties of a smoke/urban haze plume over the northeastern coast of the US, Atmos. Meas. Tech., 7, 3487-3496, https://doi.org/10.5194/amt-7-3487-2014, 2014.

Müller, D., Böckmann, C., Kolgotin, A., Schneidenbach, L., Chemyakin, E., Rosemann, J., Znak, P., and Romanov, A.: Microphysical particle properties derived from inversion algorithms developed in the framework of EARLINET, Atmos. Meas. Tech., 9, 5007-5035, https://doi.org/10.5194/amt-9-5007-2016, 2016.

Nousiainen, T. and Kandler, K.: Light scattering by atmospheric mineral dust particles. In: Kokhanovsky A. (eds) Light Scattering Reviews 9. Springer Praxis Books. Springer, Berlin, Heidelberg, 2015.

Papayannis, A., Mamouri, R. E., Amiridis, V., Remoundaki, E., Tsaknakis, G., Kokkalis, P., Veselovskii, I., Kolgotin, A., Nenes, A., and Fountoukis, C.: Optical-microphysical properties of Saharan dust aerosols and composition relationship using a multi-wavelength Raman lidar, in situ sensors and modelling: a case study analysis, Atmos. Chem. Phys., 12, 4011-4032, https://doi.org/10.5194/acp-12-4011-2012, 2012.

Pappalardo, G., Amodeo, A., Apituley, A., Comeron, A., Freudenthaler, V., Linné, H., Ansmann, A., Bösenberg, J., D'Amico, G., Mattis, I., Mona, L., Wandinger, U., Amiridis, V., Alados-Arboledas, L., Nicolae, D., and Wiegner, M.: EARLINET: towards an advanced sustainable European aerosol lidar network, Atmos. Meas. Tech., 7, 2389-2409, https://doi.org/10.5194/amt-7-2389-2014, 2014.

Shin, S.-K., Tesche, M., Kim, K., Kezoudi, M., Tatarov, B., Müller, D., and Noh, Y.: On the spectral depolarisation and lidar ratio of mineral dust provided in the AERONET version 3 inversion product, Atmos. Chem. Phys., 18, 12735-12746, https://doi.org/10.5194/acp-18-12735-2018, 2018.

Tesche, M., Ansmann, A., Müller, D., Althausen, D., Engelmann, R., Freudenthaler, V., and Groß, S.: Vertically resolved separation of dust and smoke over Cape Verde using multiwavelength Raman and polarization lidars during Saharan Mineral Dust Experiment 2008, J. Geophys. Res., 114, D13202, https://doi.org/10.1029/2009JD011862, 2009a.

Tesche, M., Ansmann, A., Müller, D., Althausen, D., Mattis, I., Heese, B., Freudenthaler, V., Wiegner, M., Eseelborn, M., Pisani, G., and Knippertz, P.: Vertical profiling of Saharan dust with Raman lidars and airborne HSRL in southern Morocco during SAMUM, Tellus B, 61, 144–164, https://doi.org/10.1111/j.1600-0889.2008.00390.x, 2009b.

Tesche, M., Groß, S., Ansmann, A., Müller, D., Althausen, D., Freudenthaler, V., and Esselborn, M.: Profiling of Saharan dust and biomass-burning smoke with multiwavelength polarization Raman lidar at Cape Verde, Tellus, 63B, 649–676, https://doi.org/10.1111/j.1600-0889.2011.00548.x, 2011a.

Tesche, M., Müller, D., Groß, S., Ansmann, A., Althausen, D., Freudenthaler, V., Weinzierl, B., Veira, A., and Petzold, A.: Optical and microphysical properties of smoke over Cape Verde inferred from multiwavelength lidar measurements, Tellus, 63B, 677-694, https://doi.org/10.1111/j.1600-0889.2011.00549.x, 2011b.

Veselovskii, I., Kolgotin, A., Griaznov, V., Müller, D., Wandinger, U., and Whiteman, D.: Inversion with regularization for the retrieval of tropospheric aerosol parameters from multi-wavelength lidar sounding, Appl. Optics, 41, 3685-3699, 2002.

Veselovskii, I., Dubovik, O., Kolgotin, A., Lapyonok, T., Di Girolamo, P., Summa, D., Whiteman, D. N., Mishchenko, M., and Tanré, D.: Application of randomly oriented spheroids for retrieval of dust particle parameters from multiwavelength lidar measurements, J. Geophys. Res., 115, D21203, https://doi.org/10.1029/2010JD014139, 2010.

Veselovskii, I., Goloub, P., Podvin, T., Bovchaliuk, V., Derimian, Y., Augustin, P., Fourmentin, M., Tanre, D., Korenskiy, M., Whiteman, D. N., Diallo, A., Ndiaye, T., Kolgotin, A., and Dubovik, O.: Retrieval of optical and physical properties of African dust from multiwavelength Raman lidar measurements during the SHADOW campaign in Senegal, Atmos. Chem. Phys., 16, 7013-7028, https://doi.org/10.5194/acp-16-7013-2016, 2016.

Weinzierl, B., Ansmann, A., Prospero, J. M., Althausen, D., Benker, N., Chouza, F., Dollner, M., Farrell, D., Fomba, W. K., Freudenthaler, V., Gasteiger, J., Groß, S., Haarig, M., Heinold, B., Kandler, K., Kristensen, T. B., Mayol-Bracero, O. L., Müller, T., Reitebuch, O., Sauer, D., Schäfler, A., Schepanski, K., Spanu, A., Tegen, I., Toledano, C., and Walser, A.: The Saharan Aerosol Long-range Transport and Aerosol-Cloud-Interaction Experiment (SALTRACE): overview and selected highlights, B. Am. Meteorol. Soc., 98, 1427–1451, https://doi.org/10.1175/BAMSD-15-00142.1, 2017.
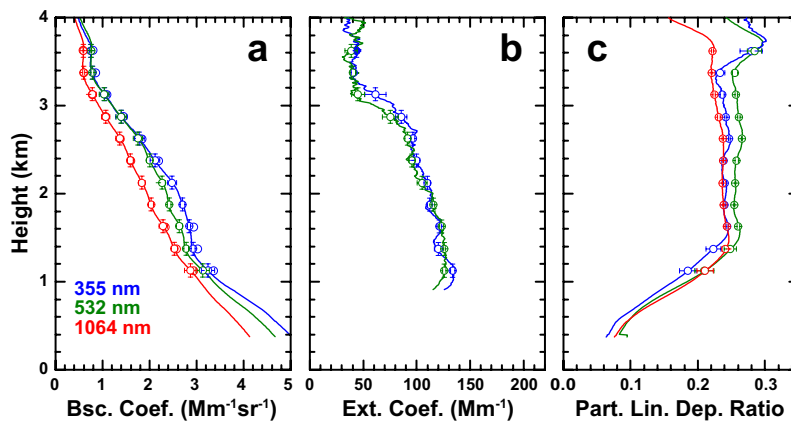
Figure 1. BERTHA measurement from 2310 to 0210 UTC on 20-21 June 2014 during SALTRACE. The measurement is representative for pure mineral dust conditions (*Haarig et al.*, 2017a). The colored circles mark the data points we used to compile the eight variations of input data sets for our data inversion (Table 2). Error bars refer to the standard deviation of the height average. Further details on this measurement are given in Table 1.
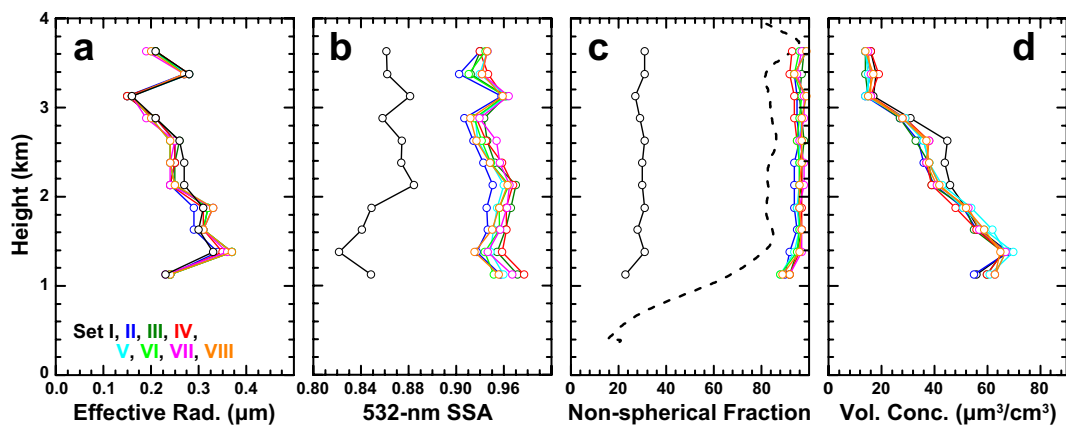
Figure 2. Inversion results of effective radius (a), 532-nm SSA (b), non-spherical fraction (c), and volume concentration (d) for eight inversion runs using the input data presented in Figure 1. The dashed line in the plot of the non-spherical fraction refers to the contribution of dust to the 532-nm backscatter coefficient that can be obtained according to the procedure described by *Tesche et al.* (2009b).
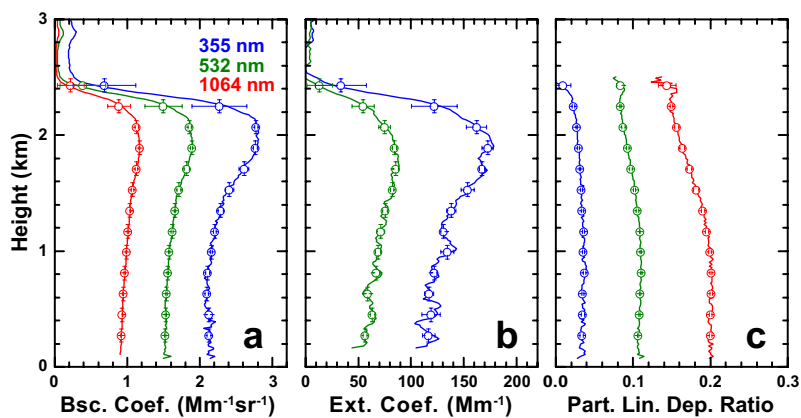
Figure 3. Same as Figure 2 but for an HSRL-2 measurement performed during the second DISCOVER-AQ Texas flight on 25 September 2013 in the vicinity of Deer Park (29.670°N, 95.128°W). The colored circles mark the data points we used to compile the inversion input data sets (Table 2). Details on the time of flight, and dust mixing ratio and aerosol types are given in Table 1.
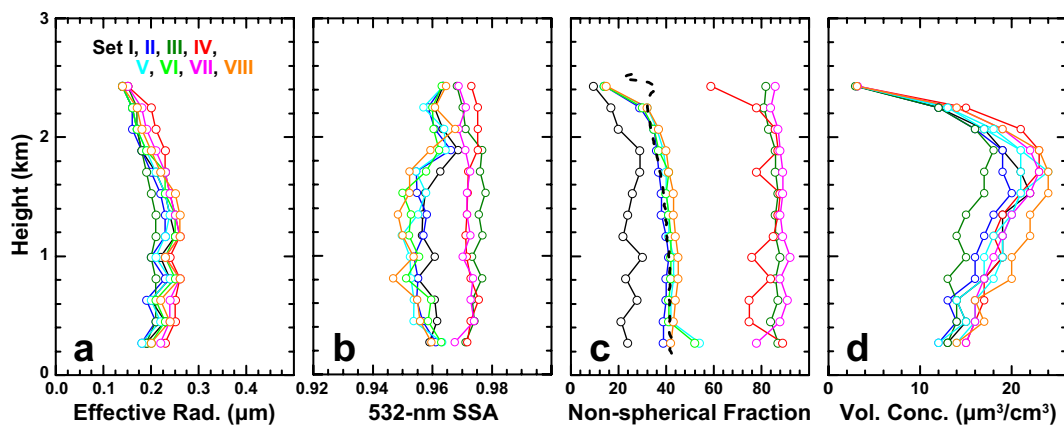
Figure 4. Same as Figure 2 but for the input data presented in Figure 3. The dashed line refers to the profile of the dust mixing ratio obtained according to *Burton et al.* (2012).
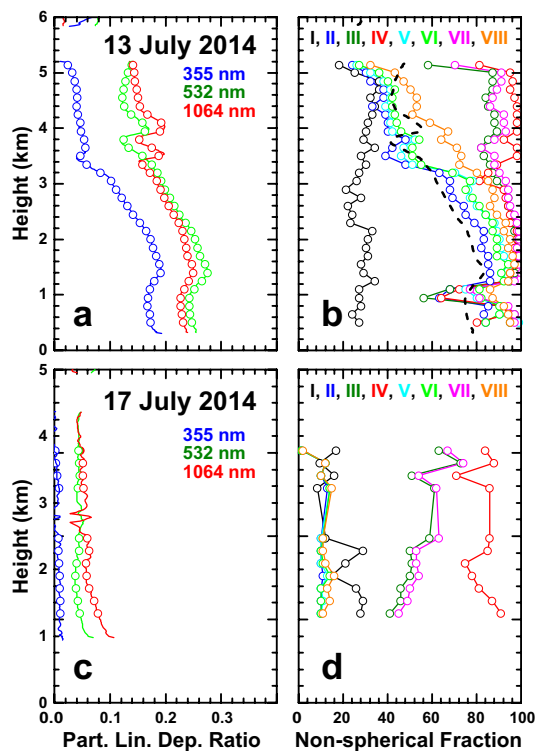
Figure 5. Profiles of (a and c) δ_λ and (b and d) the retrieved non-spherical fraction for DISCOVER-AQ Colorado flights on 13 and 17 July 2014. Note that values differ from Figure 5 in *Burton et al.* (2015) as we have used a longer averaging period of 23 minutes in our work (see Table 1).
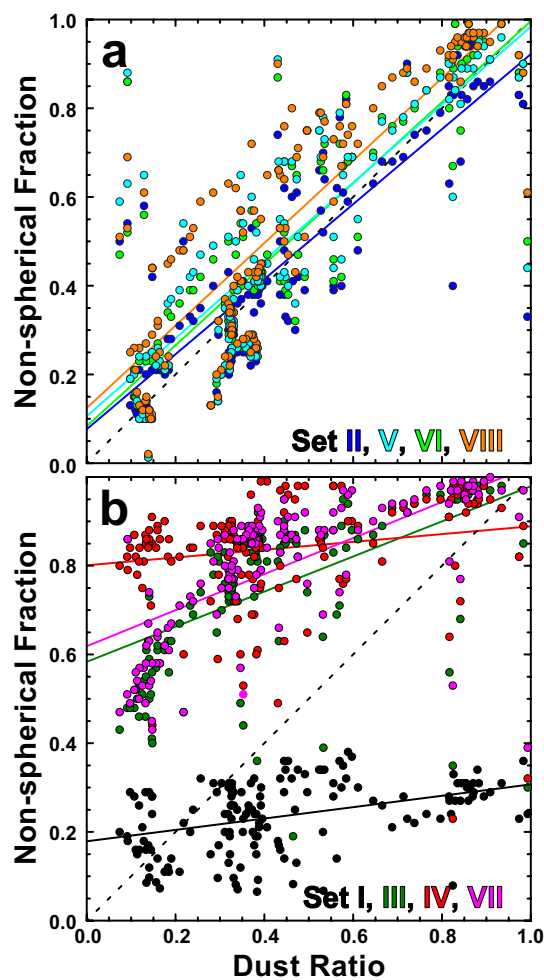
Figure 6. Connection between the retrieved fraction of non-spherical particles (from inversion) and the ratio of non-spherical particles to the 532-nm backscatter coefficient (from lidar measurements of δ_{532}) for the input data sets listed in Table 2 and the cases listed in Table 1. We split data sets according to with (a) and without (b) the use of δ_{355}, i.e. Sets II, V, VI and VIII and Sets I, III, IV and VII, respectively.
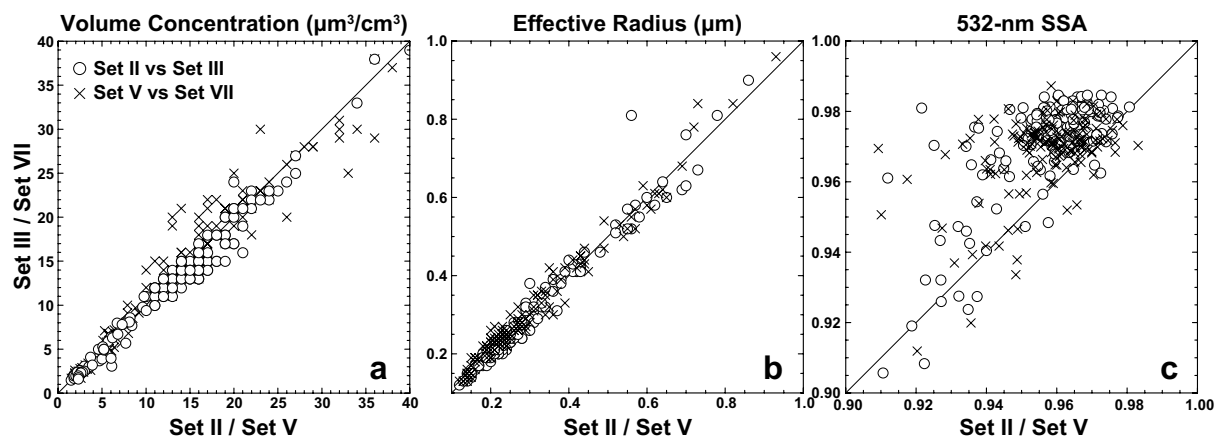
Figure 7. Correlation of inversion outputs for volume concentration (a), effective radius (b), and 532-nm SSA (c) of the 3+2+1 Sets II and III (circles) and the 3+2+2 Sets V and VII (crosses).
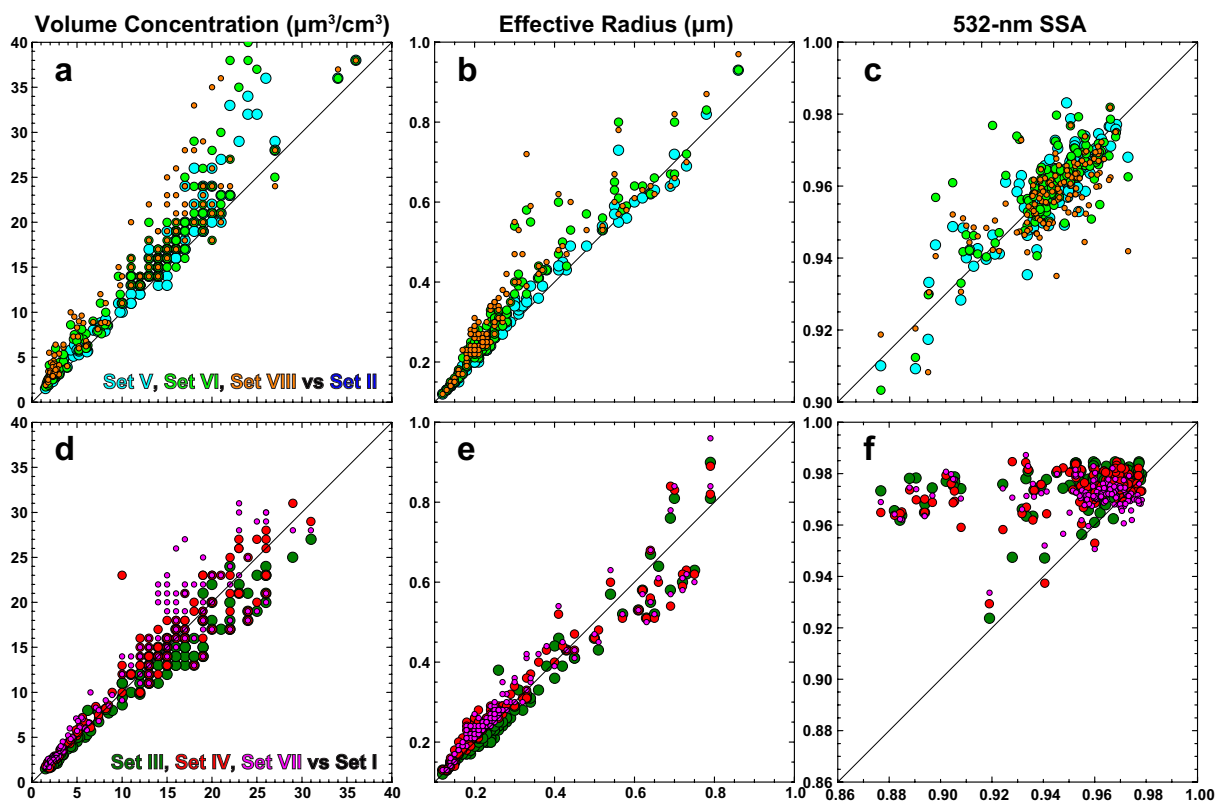
Figure 8. Same as Figure 7 but for inversion outputs with and without the use of δ_{355}. The upper row shows the correlation of Sets V, VI, and VIII to Set II while the lower row shows the correlation of Sets III, IV, and VII to Set I.

Table 1. Overview of the 3+2+3 lidar measurements taken with BERTHA and HSRL-2 and used in this study. The HSRL-2 aerosol type was determined following the procedure outlined in *Burton et al.* (2012). Note that HSRL-2 measurements include transit flights.

date	time (UTC)	height (km)	mean δ_{532}	dust ratio	aerosol type
HSRL-2: DISCOVER-AQ California (2013), Texas (2013), Colorado (2014)					
20130130	1656 - 1712	0.3 - 1.0	0.058±0.055	0.20±0.17	urban/pollution, fresh smoke
		1.0 - 1.2	0.280±0.025	0.84±0.07	dusty mix
20130208	1737 - 1802	2.0 - 2.4	0.331±0.039	0.95±0.09	dusty mix
		3.8 - 4.2	0.113±0.005	0.39±0.02	dusty mix, urban/pollution
20130925	2057 - 2105	0.3 - 2.4	0.099±0.009	0.35±0.03	dusty mix, urban/pollution
20130926	2036 - 2041	0.3 - 2.1	0.106±0.048	0.37±0.10	dusty mix, urban/pollution
20130928	1612 - 1617	0.3 - 1.9	0.045±0.007	0.17±0.03	urban/pollution
20140713	1435 - 1446	0.4 - 3.0	0.097±0.033	0.34±0.11	dusty mix, urban/pollution
	1713 - 1736	0.5 - 5.1	0.201±0.053	0.64±0.14	dusty mix
20140717	1917 - 1919	2.0 - 4.0	0.043±0.004	0.00	urban/pollution, polluted marine
20140722	2009 - 2036	2.0 - 3.0	0.183±0.010	0.59±0.03	dusty mix
		3.0 - 5.5	0.107±0.029	0.37±0.09	urban/pollution, dusty mix
BERTHA: SALTRACE, Barbados					
20140303	2230 - 2330	1.0 - 2.8	0.123±0.041	0.32±0.17	dusty mix
20140620	2310 - 0210	1.0 - 4.0	0.257±0.018	0.83±0.06	mineral dust

Table 2. Combinations of δ_λ that were used as inversion input in addition to the conventional 3+2 data set (Set I). The lower part of the table provides the slope, intercept, and squared correlation coefficients for the linear fits between dust ratio and non-spherical fraction presented in Figure 6.

data set #	I	II	III	IV	V	VI	VII	VIII
355 nm	-	X	-	-	X	X	-	X
532 nm	-	-	X	-	X	-	X	X
1064 nm	-	-	-	X	-	X	X	X
Slope	0.13	0.85	0.40	0.09	0.91	0.88	0.41	0.93
Intercept	18	8	58	80	8	11	62	13
R^2	0.16	0.68	0.33	0.03	0.73	0.68	0.46	0.73